HHS Public Access

Author manuscript

FEBS Lett. Author manuscript; available in PMC 2019 August 01.

Published in final edited form as:

FEBS Lett. 2018 August ; 592(15): 2550–2561. doi:10.1002/1873-3468.13190.

Biochemical and Structural Insights into an Allelic Variant Causing the Lysosomal Storage Disorder Aspartylglucosaminuria

Suchita Pande[1], **William Bizilj**[1], and **Hwai-Chen Guo**[1,*]

[1]Department of Biological Sciences, University of Massachusetts Lowell, 1 University Avenue, Lowell, MA 01854, USA

Abstract

Aspartylglucosaminuria (AGU) is a lysosomal storage disorder caused by defects of the hydrolase glycosylasparaginase (GA). Previously, we showed that a Canadian AGU mutation disrupts an obligatory intra-molecular autoprocessing with the enzyme trapped as an inactive precursor. Here, we report biochemical and structural characterizations of a model enzyme corresponding to a Finnish AGU allele, the T234I variant. Unlike the Canadian counterpart, the Finnish variant is capable of a slow autoprocessing to generate detectible hydrolyzation activity of the natural substrate of GA. We have determined a 1.6 Å-resolution structure of the Finnish AGU model and built an enzyme-substrate complex to provide a structural basis for analyzing the negative effects of the point mutation on K_M and kcat of the mature enzyme.

Keywords

Aspartylglucosaminuria (AGU); glycosylasparaginase (GA); autoprocessing; autoproteolysis; crystal structure; kinetic characterization

1. Introduction

Aspartylglucosaminuria (AGU) is a lysosomal storage disease which is caused by mutations in the gene encoding for an enzyme called glycosylasparaginase (GA) or aspartylglucosaminidase (AGA) [1] [EC # 3.5.1.26]. GA is involved in protein degradation by cleaving Asn-linked glycoproteins in lysosomes, and is widely distributed in vertebrate tissues [2], insect cells [3], as well as in bacteria [4]. GAs are conserved in primary sequences, tertiary structures, and activation mechanism for the hydrolase activity through an intramolecular autoproteolysis [5–9]. The enzyme is initially synthesized as an inactive

*Corresponding author: Hwai-Chen Guo, Department of Biological Sciences, University of Massachusetts Lowell, 1 University Avenue, Lowell, MA 01854, USA, telephone: 978-934-2878, fax: 978-934-3044, HwaiChen_Guo@uml.edu.
DR. HWAI-CHEN GUO (Orcid ID : 0000-0003-2664-5723)

Author Contributions

SP and HG conceived the study and designed experiments; SP and WB performed experiments; SP and HG analysed data and wrote the manuscript; SP, WB and HG made manuscript revisions.

Conflict of interest

The authors declare no conflict of interest.

single-polypeptide precursor in which α and β-subunits are joined together via a surface loop (called precursor- or P-loop) that blocks the catalytic center of the hydrolase [7]. A subsequent autoprocessing results in a main-chain cleavage at the P-loop by a self-catalyzed peptide bond rearrangement via an N → O acyl shift [10, 11]. This autoproteolysis event results in an active form of the hydrolase with separate α and β-subunits [12]. During the metabolic turnover of Asn-linked glycoproteins, autocleaved GA hydrolyzes glycoasparagine N4-(β-N-acetylglucosaminyl)-L-asparagine (NAcGlc-Asn) that connects a carbohydrate to the side chain of an asparagine [13].

Deficiency of this enzyme causes accumulation of glycoasparagines in lysosomes of cells [14], resulting in a genetic condition called aspartylglucosaminuria (AGU) [1, 15]. AGU mutations impair autoproteolysis of GA precursor and/or impair its hydrolase activity in lysosomes [16–18]. This deficiency results in progressive mental decline of the patients [19], and leads to a lifelong condition affecting patient's appearance, cognition, adaptive skills, physical growth, personality, anatomical structure, and health [1]. Early indicators of AGU include growth spurts in infants and the development of macrocephalia associated to hernias and respiratory infections [1, 20].

Close to 30 different AGU alleles have been reported around the world [13, 21, 22]. About half of these AGU alleles are independent missense mutations, the rest are frameshifts and/or polypeptide truncations/extensions. Due to a founder effect, AGU incidence in Finland is unexcelled, with one major allele (denoted AGU_{FIN}) found in 98% of the AGU patients. The AGU_{FIN} allele carries two concurrent substitutions R138Q+C140S. Mutational studies have shown that the C140S substitution is the causative mutation for GA deficiency, whereas a single mutation R138Q does not affect either GA autoproteolysis or its hydrolase activity [23]. Data also show that, in addition to preventing the disulfide bond formation between C140 and C156, the C140S substitution also causes destabilization of the unique/longer loop structure in the human sequence and thus prevent dimerization of GA essential for autoproteolytic activation [24]. Another Finnish allele, the subject of this study, has a point mutation of nucleotide C to T that changes residue 234 from a threonine to an isoleucine (named T234I variant, Table 1) [21]. Last year a new AGU variant was discovered in two male siblings in the US. Wherein, there was a large genomic deletion in the GA gene of maternal origin, while the paternal allele carried a single C to A base exchange at position 365 of the GA coding region [17]. This new AGU mutation results in substitution of Thr-122 (including the signal peptide) by a charged residue Lys (named T122K variant).

The first crystal structures of an AGU model enzyme have recently been determined by our group, corresponding a AGU allele with a single amino acid change from a glycine to an aspartic acid [16, 18]. This model enzyme (called G172D model) is reconstructed on the Flavobacteril homolog, corresponding to a Canadian AGU allele named in the literature as either G203D or G226D variant; these numbering differences are due to omitting or including the signal peptide, as well as different lengths of the P-loop that connects α and β subunits in the precursors (Table 1). The structural studies revealed that the G172D model variant appears to cause local conformational change, which in turn disrupts the requisite autoprocessing step to generate metabolically functional mature hydrolase. Nonetheless, vast biochemical information in the literatures indicate that each AGU variant behaves differently

in regard to autoprocessing, substrate hydrolysis, and/or thermal stability [13, 21], suggesting that detailed structural and catalytic consequences of different AGU variants could vary widely. For example, inherent to the Canadian AGU allele, the point mutation is located outside of the hydrolase substrate site, and thus does not have direct impact on the downstream hydrolase activity. Instead, it causes a local conformational change at the autoprocessing site, subsequently trapping the protein in the inactive precursor form. On the other hand, the second Finnish mutation (T234I variant) is located at the rim of the substrate binding site, and its precursor appears to have a detectible level of autoprocessing capability [16]. Such dissimilitude between these variants points to the need for more structural and biochemical characterizations of other AGU variants. In this study, we generated another AGU model enzyme, named T203I model (Table 1), corresponding to the Finnish allele T234I variant. This model enzyme allows us to study the detailed biochemical and structural consequences of this particular AGU variant. Results indicate that replacement of the conserved threonine with an isoleucine has negative impacts on both K_M and, to a greater extent, kcat of hydrolase activity. We also report here a 1.6 Å-resolution crystal structure to enable structure-function analyses of the second Finnish AGU mutated hydrolase.

2. Materials and Methods

2.1. Protein expression and purification

Wild-type GA and AGU T203I variant proteins, constructed on a Flavobacterial homolog, were over-expressed and purified using previously published protocols [25].

2.2. Hydrolase activity assay

Hydrolase activity was measured by a method modified from a previously described approach [26]. To monitor hydrolase activity of *in vitro* autoprocessed samples, purified protein was incubated at 37°C to initiate the autoproteolysis in a buffer solution of 100mM Tri, pH 7.5, 50 mM NaCl, 10 mM EDTA. At various time points, 50μl of *in vitro* autoprocessed protein samples were removed to add aspartic acid β-(p-nitroanilide) to a final concentration of 1.5 mM in a 100μl reaction mixture, which was then incubated at 37°C for an additional hour. The release of p-nitroaniline was subsequently monitored at 405nm using Spectramax-M2 spectrophotometer.

The K_M and k_{cat} values of wild-type and variant T203I were determined by measuring the release of NAcGlc (*N*-acetylglucosamine) using NAcGlc-Asn as substrates. A series of reactions were set up in 13 different concentrations of NAcGlc-Asn from 0.001 to 0.5 mM. Each reaction was in 20 μl of 20 mM sodium phosphate buffer, pH 7.5, incubated with 0.04–0.08 ug of enzyme for an appropriate time at 37 °C [27]. The reactions were stopped by adding 50 μl of 250 mM sodium borate buffer, pH 8.8, followed by boiling for 3 min. Released of NAcGlc was assayed by the Morgan-Elson reaction [28].

2.3. Crystallization and data collection

Hanging-drop vapor diffusion technique was used in the initial crystallization screenings. Needle-like crystals of the T203I variant grew in the screens using purified variant protein. Micro-seeding method was used to improve crystal quality. The best looking crystals were

formed above a well solution containing 0.2M NaCl, 0.1M Bis-Tris pH 6.5, 25% PEG 3350, and a protein concentration of 2mg/ml.

For data collection, the crystal was cryoprotected in solution containing 100 mM Tris-HCl buffer pH 8.0 and 20% glycerol. X-ray data were collected at 100K using the beamline X29 at the National Synchrotron Light Source (NSLS), Brookhaven National Laboratory. The data were processed with the Mosflm29 and the CCP4 suite [29]. The crystal has $P2_1$ symmetry with two protein molecules in the asymmetric unit.

2.4. Structure determination and refinement

The structures of T203I variant were determined by molecular replacement method, using the previously published structure of the GA wild-type enzyme (PDB code 2GAW) as the starting model [6]. To avoid model bias, the initial MR phases were calculated by omitting several residues juxtaposing the T203I substitution, residues 200–206. Molecular replacement was performed with Molrep and refinements were carried out with the Refmac program, with 5% of the total reflection data excluded from the beginning of refinement cycles and later used to calculate the free R-factor (R_{free}) for monitoring refinement progress. This partial model was further subjected to rigid body and restrained refinements, with model rebuilding done in COOT [30] to obtain the final structure. The final model contains 285 residues (2-142, 152-295) in molecule 1 and 281 residues (2-138, 152-295) in molecule 2, and 224 water molecules, and is refined to crystallographic R_{work}/R_{free} of 16.9%/19.7% at 1.6 Å resolution. The X-ray data collection, processing, and structure refinement statistics are summarized in Table 2. All the figures were drawn using PyMOL (DeLano Scientific) and labels were added using Adobe® Photoshop.

2.5. Complex model building

T203I-NAcGlc-Asn complex was generated by superimposing secondary structure of T203I mature structure with the previously published T152C GA-NAcGlc-Asn complex (GA-substrate structure, PDB code 2GL9) [31]. The coordinates of the NAcGlc-Asn substrate were then placed into the substrate binding site of current apo-T203I structure.

2.6. Protein Data Bank accession codes

The atomic coordinates and structure factors have been deposited in the Protein Data Bank under the accession number 6DEY.

3. Results

3.1. Generation of a T203I variant as a model enzyme for the AGU T234I variant

Studies of AGU variants in human GA is hindered due to difficulty in obtaining sufficient amounts of recombinant enzyme for *in vitro* biochemical or structural analyses [32]. A HeLa culture system has been reported recently for biochemical and cellular characterization of human AGU variants [17]. But it is not likely to produce crystallographic amount of purified protein for structural studies. In contrast, a Favobacterial system has been shown to be an excellent model system for these studies. The Flavobacterium GA shares the same αββα fold as the human enzyme [5–7, 33]. The human and Flavobacterial GA share highly

significant sequence homology, with an overall 36% identity plus 53% conserved similarity, and an Expect value 1e-48 in BLAST [34]. They both utilize the autoproteolytic process to cleave the single-chain precursor in order to form the mature form for the hydrolase activity [8, 35]. More importantly, all the amino acids around the catalytic center, those within 4 Å of the bound substrate NAcGlc-Asn, are 100% identical between these two enzymes [31], suggesting suitability of using the Flavobacterium homolog to study effects of AGU mutations on GA catalysis. To this end, we employed an MBP-GA fusion protein expression system that allowed us to obtain highly purified protein in crystallographic amounts [25]. Taking advantage of this recombinant system, we have generated a model enzyme to analyze consequence of a Finnish AGU allele, the T234I variant, on GA structure and functions. According to the structure-based alignments [6], Thr203 in Flavobacterium GA is equivalent to Thr234 in human counterpart. We had thus generated an AGU model with a Thr-to-Ile substitution at residue 203 of Flavobacterium GA, named T203I variant (Table 1), as a model enzyme to study the Finnish T234I AGU allele. T203I model and wild-type (WT) enzyme were purified according to the previously described protocols [25].

3.2. Hydrolase activities of the T203I model enzyme

Purified T203I variant protein was first characterized by its autoproteolytic and hydrolytic activities, and compared them to the WT enzyme. As shown in Fig. 1A, WT GA autoproteolyzed spontaneously into the functional mature form with the α and β subunits. In contrast, the purified T203I variant remained as a single-chain precursor, indicating a deficiency in its autoproteolytic processing. The hydrolytic activities of the T203I variant was also examined using a substrate analog, aspartic acid β-(p-nitroanilide). Hydrolysis was then monitored by measuring absorbance at 405nm for the hydrolysis product, p-nitroalinine. As expected from the autoproteolysis analysis above (Fig. 1A), T203I has a negligible hydrolysis activity since it stayed mainly as an inactive precursor, ~1% as compared to that of the WT enzyme (Fig. 1B).

3.3. Structure determination of the T203I variant

To study the effects of the Thr to Ile point mutation on enzyme structure, we carried out structure determination of the T203I variant by X-ray crystallography. To this end, purified T203I protein was subject to multiple crystallization screens. Some initial conditions gave promising needle-like crystals, which were further improved by micro- and macro-seeding techniques to obtain diffracting quality crystals. Before X-ray data collection, crystals were soaked with 20% glycerol as a cryo-protectant for data collection at 100K. Crystal structure of the T203I variant has now been determined and refined to 1.6 Å resolution. The space group and cell constants of T203I crystals are: $P2_1$, a = 45.9, b = 96.5, c = 61.7 Å; β = 90.3°, with an Rfree of 0.197 and a Rwork of 0.169. Other crystallographic statistics are summarized in Table 2.

Although protein samples of T203I used for crystallization are essentially in the precursor form (Fig. 1A), electron density maps calculated from the diffraction data clearly indicated that the P-loop (residues 142–151) linking α and β subunits in the precursor had been autocleaved into the mature form in both molecules of the asymmetric unit (Fig. 2). This crystallographic interpretation is based on quality of electron density (Fig. 2), as well as

real-space correlation coefficient (0.94) and B factor (13.9 $Å^2$) for the autocleaved N-terminal amino group at Thr-152, and comparing various type of difference and omit maps with various contour levels [29]. Figure 2B shows a contrast between the well resolved density at Thr-152 of the autocleaved T203I, and the continuous density for the P-loop (Asn149-Thr152) of a precursor variant [16]. In the T203I structure (Fig 2B, left panel), a surface loop (Arg49-Gly54) moves closer to Thr152, suggesting the P-loop had been autocleaved and released out of the space. Altogether, the results indicates that the T203I variant was able to slowly undergo autoproteolysis over the several days' process of crystal growth. Previously we have shown that precursor and mature forms of GA would grow into different forms of crystals in the space groups P1 and $P2_1$, respectively [25]. We have also shown that some GA variants could grow P1 crystals as precursors, but then slowly autoproteolyzed into the mature form inside the P1 crystals [16, 18]. However, the T203I variant crystallized in the $P2_1$ space group, suggesting that this variant protein was first autoproteolyzed in solution during several days' crystallization process, before growing into the $P2_1$ mature form crystals. We previously also showed that GA dimerization is essential to facilitate the autoprocessing of protein precursor [24]. This notion is consistent with a recent report that co-expression of WT GA can reduce the autoprocessing defect of some AGU variants [17], suggesting inter-molecular interactions are involved in the autoactivation. It is thus plausible that the autoproteolysis of the T203I precursor could have been facilitated by its attachment onto the $P2_1$ crystal surface, resulting in addition of an autoproteolyzed/mature T203I molecule onto the growing $P2_1$ crystal (which could only pack mature form protein).

3.4. Structural comparisons between the autocleaved T203I and the wild-type GA enzyme

Structures of the mature T203I and the wild-type (WT) GA enzymes (PDB code 2GAW) [6] were compared to study effects of the Thr to Ile point mutation on enzyme structure. Overall, structure of the T203I variant is very similar to that of WT enzyme, with the typical αββα-sandwich fold. The rmsd of all main-chain atoms of 275 residues is 0.24 Å, indicating a well-folded GA protein with no gross conformational changes or misfolding. Interestingly, the main-chain trace of the mutated residue 203 is also very similar to the WT GA, with an average displacement of 0.18 Å. The similarity in structure highlights the only change from a hydroxyl to an ethyl group in the T203I variant, thus confirm the critical role of the hydroxyl group of Thr-203 (see below). There are however small local shifts observed, by an average of 0.322 Å and 0.429 Å deviations in residues 133-138 and 286-290, respectively. These shifts do not appear to be due to the T203I mutation since they are more than 23 and 10 Å away from the mutated residue, respectively, thus make no direct contact. Both shifted segments are located at the C-terminal ends of the α and β subunits, respectively. These small but significant displacements appear to be due to a static disorder or dynamic flexibility, indicated by an elevated B factors (23.15 $Å^2$ vs an overall average of 11.6 $Å^2$). Throughout the structures, there are two peptide bonds flipped when compared to the WT structure, at residues Tyr53 and Ile187; these flips are plausible since both peptide bonds are followed by a glycine residue, thus with less structural constraints. Similar to the apo-structure of the WT enzyme, the T203I variant acquires a wide opening near the substrate-binding site [6]. This suggests that T203I has its substrate-binding site fully opened through the autoproteolysis and is ready to accommodate the substrate NAcGlc-Asn.

3.5. Slow autoactivation of the T203I variant

The initial autoproteolysis analyses (Fig. 1A) indicates that the T203I variant remains primarily as a single-chain precursor, even after two-days' protein purification process at 4°C (Fig. 1A). Consistent with results in the literature [21], this finding indicates the T203I variant is deficient in autoactivation. Nonetheless, x-ray diffracting data clearly showed that mutated enzyme inside the crystals is mainly in its autoprocessed form with autocleaved α and β subunits (see above). Together, these results suggest that the T203I variant is still capable of autoprocessing into the mature form over the several days' process of crystal growth. To analyze this slower autoprocessing activity of the T203I variant, we monitored its progress by incubating the purified T203I variant protein at 37°C for up to 32 hours, and analyzed its autocleavage by the SDS-PAGE (Fig. 3A). Meanwhile samples at corresponding time-points of the thermal incubation are also assayed for their hydrolase activities (Fig. 3B). As shown in Fig. 3A, the T203I precursor was able to slowly autoproteolyze into the mature form with the α and β subunits. The $t_{1/2}$ of autoproteolysis for the T203I variant is ~4 hours, compared to < 1 min for the WT [35]. Meanwhile, there is a small but significant increase of hydrolase activities for the T203I variant, ~7% of the wild-type activity after 16-hr *in vitro* autoactivation (Fig. 3B), correlating to a concurrent increase of the autocleaved variant protein (Fig. 3A). In Figure 3B, the t score is 9.46 with a p-value 0.0007 when comparing the 16-hr activities of T203I variant with the 0-hr control. In contrast, the wild-type GA actually had a small decrease of hydrolase activities over the same period of time, probably due to a thermal denaturation. Further incubation at 37°C beyond 32 hours resulted in a loss of hydrolase activity for both the wild-type and the T203I variant, again likely due to enzyme denaturation and/or degradation during the thermal incubation.

3.6. Kinetic characterization of the T203I variant and wild-type enzyme

As shown in Figure 3A, vast majority of T203I variant precursor was able to complete autoprocessing after 16-hr thermal incubation. This allows us to prepare T203I mature enzyme for measuring kinetic parameters of its hydrolysis activity. As demonstrated in Figure 1A (lane $T203I_{+16}$), after 16-hour *in vitro* thermal incubation, vast majority of T203I precursor had been converted into the mature form with the α and β subunits. There was however a residual fraction of sample recalcitrant to autoprocessing into the mature enzyme even with a longer incubation, probably due to thermal denaturation (Figs. 1A and 3A).

Using the *in vitro* autoprocessed sample of the T203I variant shown in Figure 1A, we carried out kinetic studies of the mature form of T203I variant and compared them to the WT GA. Kinetic parameters K_M and k_{cat} of the variant and WT GA were determined using the natural substrate NAcGlc-Asn. Typical kinetic analyses of the initial rates as a function of substrate concentration are shown in Figure 4. Wild-type enzyme had a K_M for the natural substrate NAcGlc-Asn of 0.090 mM, and the *k*cat was 14.18 s^{-1}. These kinetic parameters are similar to previously reported values for human and bacterial GA [28, 36]. Substitution of the Thr-203 by Ile greatly reduced the enzyme activities; both K_M and *k*cat were adversely affected (Table 3). The T203I variant had about 200-fold decreases in the *k*cat. Relative to WT enzyme, the K_M of T203I variant for the natural substrate was much less affected than *k*cat, by only about two-fold. As a result, the specificity constant (*k*cat/K_M) of T203I variant was decreased by more than 300-fold when compared to the WT GA.

3.7. A T203I-substrate complex model for structural analyses

As demonstrated in the SDS-PAGE above (Fig. 3A), T203I variant is capable of autoprotolysis. However, the autoprocessed variant only has a low level of hydrolase activity when compared to the WT enzyme. To analyze structural basis for the deficiency of T203I variant in hydrolysis, we modeled a T203I-substrate complex based on previously published structure of the WT GA-substrate complex (2GL9) [31]. After a superimposition by all the secondary structure elements, the substrate model from the WT-substrate complex was placed into the apo-T203I variant enzyme structure, to build the T203I-substrate complex structure. In this complex model (Fig. 5A), T203I has a slightly wider substrate-binding site. Such a wide opening resembles the so-called “open conformation” that was also observed in the apo-WT GA structure [6]. However, for the WT enzyme, binding of a substrate molecule resulted in a narrower substrate site, called “closed conformation” [31] (Fig. 5A). In the T203I-substrate complex model, all the previously identified substrate binding residues (W11, F13, S50, T152, R180, D183, G204, G206) are in close contact distances (less than 4 Å) from the substrate model, except the mutated residue Ile203 (Fig. 5A).

Previously we have proposed that during hydrolysis of the substrate by the WT GA, the side-chain hydroxyl group of Thr203 makes a hydrogen-bond contact with the carbonyl oxygen atom of the substrate, to serve as the oxyanion hole to stabilize the reaction intermediate [31]. However, as shown in Fig. 5A, substitution of the Thr-203 with an isoleucine in the T203I variant would prevent such hydrogen-bond interactions into the “closed conformation” to grasp the substrate. As a result, substrate hydrolysis is impeded even after prolonged incubation at 37°C (Fig. 3B), likely due to the lack of an appropriate oxyanion hole to stabilize the hydrolysis intermediate.

On the other hand, although the *k*cat values were adversely affected, small but detectible reaction rates remained for the T203I mature variant. It thus appears that the variant-substrate complex is still capable of hydrolyzing the substrate slowly through a negatively charged transition state. But the mutation of Thr-203 to a non-polar side chain Ile appears to abolish the original hydrogen-bond networking proposed for the oxyanion hole for stabilizing the negatively charged reaction intermediate. To explain this low hydrolase activity, we found, within the crystal structure of the variant enzyme, a nearby bound water molecule that might fill in the role of the oxyanion hole. In the crystal structure, a bound water molecule (#217) is located near the mutated Ile-203 (Fig. 2A). Upon substrate binding to the variant enzyme, this water molecule could probably adjust slightly to form a hydrogen-bonding interaction (~2.6 Å) with the scissile carbonyl oxygen of the substrate (Fig. 5B). Thus during the substrate hydrolysis by the T203I variant, this modeled water molecule could be polarized to stabilize the negatively charged transition state. However, even though the water molecule is located at an appropriate distance from the scissile carbonyl, it is tilted away (by50°) from the carbonyl direction and therefore is not with an ideal geometry to serve as an optimal oxyanion hole. This might explain why the T203I variant is still capable of hydrolysis, but with a greatly reduced kcat.

4. Discussion

Defective GA is produced in AGU patients due to various missense mutations or deletions, mostly in the Finnish population but also found in other parts of the world. These variants affect the activity of GA either by preventing its autoprotolysis activity and/or by affecting hydrolysis of its natural substrate NAcGlc-Asn. In this study, the T203I variant, which is a model enzyme for the Finnish AGU T234I variant, was found to be defective in its autoproteolysis and is thus purified as an inactive single-chain precursor. We have previously showed that GA precursor protein has structural constraints near the scissile peptide bond at Thr152, with presumably a less stable conformation [7, 9, 37]. It thus requires a break by autoprocessing at the scissile peptide-bond to relieve these structural constraints, for conversion to a more energetically stable conformation. It is plausible that the T203I mutation results in a less constrained precursor conformation and therefore was trapped in the pre-autoproteolysis precursor form [37]. This has been shown to be the case for another Canadian AGU model G172D [16]. Structural studies of the T203I precursor protein are necessary to confirm the lack of structural constraints as the cause of autoproteolysis deficiency for the Finnish AGU variant.

This study also showed that the T203I variant precursor is still capable of a slow *in vitro* autoprocessing into its mature form (Figure 3A), consistent with previously published data [16]. Such a slow autoprocessing can happen either after several days' crystallization at 4°C, or by several hours' thermal incubation at 37°C. Furthermore, hydrolysis activity of the T203I variant appears to correlate with the amount of autocleaved T203I protein. Hence, it appears that even though with a lower level of hydrolase activity relative to the wild-type enzyme, the T203I variant is still capable of hydrolyzing the natural NAcGlc-Asn substrate once the enzyme is autocleaved into the mature form. As demonstrated in this study (Figure 1A and Sections 3.5 & 3.6), one would need to be very careful about whether the kinetic studies of GA or AGA hydrolysis are carried out using the mature form of enzyme. Even though some kinetic characterization of a T203A variant had been reported before [28], it appears that those data were based on its purified precursor protein, making data interpretation complicated. In this study, we have characterized kinetic parameters of this mature T203I enzyme. Data indicate that replacement of the conserved Thr-203 with a nonpolar side chain of isoleucine has negative impacts on both K_M and kcat. The T203I variant had about 200-fold decreases in *k*cat, whereas the K_M of T203I variant was increased to about two-fold relative to wild-type enzyme. All together, the specificity constant (*k*cat/K_M) of T203I variant was reduced by more than 300-fold relative to the wild-type GA.

To study the mechanistic consequences of the Thr to Ile mutation, a T203I-substrate complex model was generated. Residues W11, F13, S50, T152, R180 and D183 of the variant all interact with the substrate similarly to the WT enzyme [31]. Figure 5A shows the most significant interactions of the T203I and WT GA with the substrate molecule. In the variant complex model, residue G204 and I203 acquired a wider opening (in the "open conformation") as compared to the WT-substrate complex (in the "closer conformation"). For the wild-type GA, the proposed catalytic reaction mechanism of a substrate processing is initiated by a Thr152 nucleophilic attack. The negatively charged intermediate is stabilized by an oxyanion hole which is likely comprised of the hydroxyl group of Thr-203

and main-chain nitrogen of Gly-204. For the T203I variant, after substrate binding, even if main-chain nitrogen of Gly-204 can interact with the substrate, the side chain of Ile-203 lacks a hydroxyl group to make a hydrogen-bond contact and grasp the substrate into the "closed conformation". As a result, the hydrogen-bond network seen in the WT-substrate complex to serve as the oxyanion hole is impaired. Nonetheless, presence of a nearby water molecule (adjusted from the bound water# 217, Fig. 5B) might fill in the gap for a partial stabilization of the reaction intermediate. This would explain the residual hydrolysis activity of this variant after it becomes autoproteolyzed *in vitro*. The complex structure model also correlated well with the kinetic analyses using the NAcGlc-Asn as substrate. The T203I variant showed an about 2-fold increase in K_M with a more dramatic 200-fold reduction of *k*cat. The relatively small change in K_M by this variant appears to result from inability of the non-polar Ile-203 side-chain to grasp the substrate into the "closed" conformation. On the other hand, the more dramatic reduction in kcat is consistent with the proposed mechanism utilizing side-chain hydroxyl of the conserved Thr-203 to serve as the oxyanion hole. These results are consistent with previous studies on T203A variant [28]. All these variants had more dramatic impacts on kcat than K_M, confirming the roles of Thr-203 in substrate hydrolysis more than on substrate binding.

Small molecule activators have been described to be able to enhance autoprocessing of certain AGU-like variant precursors that were trapped in the inactive precursor form due to some local misfolding. For example, glycine was reported to be able to increase the autoprocessing of a GA D151G variant, resulting in a significant increase of hydrolase activity [35]. Similarly, glycine and Betaine had been identified as small molecules that are capable of enhancing autoprocessing of an US AGU variant T122K or the AGU_{FIN} variant [17]. Thus, small molecule activators appear to be promising agents to treat autoprocessing deficiency of some AGU-variants. However, it is worth noting that this approach might not be suitable for other types of AGU variants. For example, some AGU mutations result in a truncated polypeptide, which would need to be rescued by reagents other than an autoproteolysis activator [38]. Furthermore, mutations at the catalytic site, such as the T203I variant studied in this report, would likely require more than an autoprocessing activator to rescue its defective oxyanion hole for substrate hydrolysis. Further studies are essential to fine-tune appropriate treatments for different types of AGU variants.

Acknowledgments

We thank Dr. Howard Robinson for assistance on data collection, Damodharan Lakshminarasimhan for the initial crystallization screens and data collections. This work was supported by Grant DK075294 from the NIH.

Abbreviations

AGU	aspartylglucosaminuria
AGA	aspartylglucosaminidase
GA	glycosylasparaginase
NAcGlc	*N*-acetylglucosamine

NAcGlc-Asn	N4-(β-N-acetylglucosaminyl)-L-asparagine
Ntn	N-terminal nucleophile
rmsd	root mean square deviation/displacement

References

1. Arvio M, Mononen I. Aspartylglycosaminuria: a review. Orphanet journal of rare diseases. 2016; 11:162. [PubMed: 27906067]
2. Tollersrud OK, Aronson NNJ. Comparison of liver glycosylasparaginases from six vertebrates. Biochem J. 1992; 282(Pt 3):891–7. [PubMed: 1554372]
3. Liu Y, Dunn GS, Aronson NNJ. Purification, biochemistry and molecular cloning of an insect glycosylasparaginase from Spodoptera frugiperda. Glycobiology. 1996; 6:527–36. [PubMed: 8877373]
4. Tarentino AL, Plummer THJ. The first demonstration of a procaryotic glycosylasparaginase. Biochem Biophys Res Commun. 1993; 197:179–86. [PubMed: 8250923]
5. Oinonen C, Tikkanen R, Rouvinen J, Peltonen L. Three-dimensional structure of human lysosomal aspartylglucosaminidase. Nat Struct Biol. 1995; 2:1102–8. [PubMed: 8846222]
6. Guo H-C, Xu Q, Buckley D, Guan C. Crystal structures of Flavobacterium glycosylasparaginase: an N- terminal nucleophile hydrolase activated by intramolecular proteolysis. J Biol Chem. 1998; 273:20205–12. [PubMed: 9685368]
7. Xu Q, Buckley D, Guan C, Guo H-C. Structural insights into the mechanism of intramolecular proteolysis. Cell. 1999; 98:651–61. [PubMed: 10490104]
8. Saarela J, Oinonen C, Jalanko A, Rouvinen J, Peltonen L. Autoproteolytic activation of human aspartylglucosaminidase. Biochem J. 2004; 378:363–71. [PubMed: 14616088]
9. Wang Y, Guo H-C. Crystallographic snapshot of glycosylasparaginase precursor poised for autoprocessing. J Mol Biol. 2010; 403:120–30. [PubMed: 20800597]
10. Perler FB. Breaking up is easy with esters. Nat Struct Biol. 1998; 5:249–52. [PubMed: 9546209]
11. Paulus H. Protein splicing and related forms of protein autoprocessing. Annu Rev Biochem. 2000; 69:447–96. [PubMed: 10966466]
12. Guan C, Cui T, Rao V, Liao W, Benner J, Lin CL, Comb D. Activation of glycosylasparaginase: formation of active N-terminal threonine by intramolecular autoproteolysis. J Biol Chem. 1996; 271:1732–7. [PubMed: 8576176]
13. Aronson NNJ. Aspartylglycosaminuria: biochemistry and molecular biology. Biochimica et biophysica acta. 1999; 1455:139–54. [PubMed: 10571008]
14. Maury CP. Accumulation of glycoprotein-derived metabolites in neural and visceral tissue in aspartylglycosaminuria. J Lab Clin Med. 1980; 96:838–44. [PubMed: 7419967]
15. Aula P, Jalanko A, Peltonen L. Aspartylglucosaminuria. In: Scriver CR, Beaudet AL, Sly WS, Valle D, Childs B, Vogelstein B, Kinzler KW, editorsThe Metabolic and Molecular Bases of Inherited Disease. McGraw-Hill; New York, USA: 2001. 3535–50.
16. Sui L, Lakshminarasimhan D, Pande S, Guo H-C. Structural Basis of a Point Mutation that Causes the Genetic Disease Aspartylglucosaminuria. Structure. 2014; 22:1855–61. [PubMed: 25456816]
17. Banning A, Gulec C, Rouvinen J, Gray SJ, Tikkanen R. Identification of Small Molecule Compounds for Pharmacological Chaperone Therapy of Aspartylglucosaminuria. Scientific reports. 2016; 6:37583. [PubMed: 27876883]
18. Pande S, Lakshminarasimhan D, Guo H-C. Crystal structure of a mutant glycosylasparaginase shedding light on aspartylglycosaminuria-causing mechanism as well as on hydrolysis of non-chitobiose substrate. Mol Genet Metab. 2017; 121:150–156. [PubMed: 28457719]
19. Arvio P, Arvio M. Progressive nature of aspartylglucosaminuria. Acta Paediatr. 2002; 91:255–7. [PubMed: 12022293]

20. Arvio P, Arvio M, Marttinen E, Sipila I, Pirinen S. Excessive infantile growth and early pubertal growth spurt: typical features in patients with aspartylglycosaminuria. J Pediatr. 1999; 134:761–3. [PubMed: 10356147]
21. Saarela J, Laine M, Oinonen C, Schantz C, Jalanko A, Rouvinen J, Peltonen L. Molecular pathogenesis of a disease: structural consequences of aspartylglucosaminuria mutations. Hum Mol Genet. 2001; 10:983–95. [PubMed: 11309371]
22. Opladen T, Ebinger F, Zschocke J, Sengupta D, Ben-Omran T, Shahbeck N, Moog U, Fischer C, Burger F, Haas D, Ruef P, Harting I, Al-Rifai H, Hoffmann GF. Aspartylglucosaminuria: unusual neonatal presentation in qatari twins with a novel aspartylglucosaminidase gene mutation and 3 new cases in a Turkish family. J Child Neurol. 2014; 29:36–42. [PubMed: 23271757]
23. Ikonen E, Enomaa N, Ulmanen I, Peltonen L. In vitro mutagenesis helps to unravel the biological consequences of aspartylglucosaminuria mutation. Genomics. 1991; 11:206–11. [PubMed: 1765378]
24. Wang Y, Guo H-C. Two-step dimerization for autoproteolysis to activate glycosylasparaginase. J Biol Chem. 2003; 278:3210–9. [PubMed: 12433919]
25. Cui T, Liao P-H, Guan C, Guo H-C. Purification and crystallization of precursors and autoprocessed enzymes of Flavobacterium glycosylasparaginase: an N-terminal nucleophile hydrolase. Acta Crystallogr D Biol Crystallogr. 1999; 55:1961–4. [PubMed: 10531509]
26. Tollersrud OK, Aronson NN Jr. Purification and characterization of rat liver glycosylasparaginase. Biochem J. 1989; 260:101–8. [PubMed: 2775174]
27. Levvy GA, McAllan A. The N-acetylation and estimation of hexosamines. Biochem J. 1959; 73:127–32. [PubMed: 14416360]
28. Liu Y, Guan C, Aronson NNJ. Site-directed mutagenesis of essential residues involved in the mechanism of bacterial glycosylasparaginase. J Biol Chem. 1998; 273:9688–94. [PubMed: 9545303]
29. Winn MD, Ballard CC, Cowtan KD, Dodson EJ, Emsley P, Evans PR, Keegan RM, Krissinel EB, Leslie AG, McCoy A, McNicholas SJ, Murshudov GN, Pannu NS, Potterton EA, Powell HR, Read RJ, Vagin A, Wilson KS. Overview of the CCP4 suite and current developments. Acta Crystallogr D Biol Crystallogr. 2011; 67:235–42. [PubMed: 21460441]
30. Emsley P, Cowtan K. Coot: model-building tools for molecular graphics. Acta Crystallogr D Biol Crystallogr. 2004; 60:2126–32. [PubMed: 15572765]
31. Wang Y, Guo H-C. Crystallographic snapshot of a productive glycosylasparaginase-substrate complex. J Mol Biol. 2007; 366:82–92. [PubMed: 17157318]
32. Saarela J. PhD Thesis. University of Helsinki; Helsinki, Finland: 2004. Characterization of aspartylglucosaminidase activation and aspartylglucosaminuria mutations.
33. Oinonen C, Rouvinen J. Structural comparison of Ntn-hydrolases. Protein Sci. 2000; 9:2329–37. [PubMed: 11206054]
34. Tatusova TA, Madden TL. BLAST 2 Sequences, a new tool for comparing protein and nucleotide sequences. FEMS Microbiol Lett. 1999; 174:247–50. [PubMed: 10339815]
35. Guan C, Liu Y, Shao Y, Cui T, Liao W, Ewel A, Whitaker R, Paulus H. Characterization and functional analysis of the cis-autoproteolysis active center of glycosylasparaginase. J Biol Chem. 1998; 273:9695–702. [PubMed: 9545304]
36. Kaartinen V, Williams JC, Tomich J, Yates JRr, Hood LE, Mononen I. Glycosaparaginase from human leukocytes: inactivation and covalent modification with diazo-oxonorvaline. J Biol Chem. 1991; 266:5860–9. [PubMed: 2005122]
37. Qian X, Guan C, Guo H-C. A dual role for an aspartic acid in glycosylasparaginase autoproteolysis. Structure. 2003; 11:997–1003. [PubMed: 12906830]
38. Banning A, Schiff M, Tikkanen R. Amlexanox provides a potential therapy for nonsense mutations in the lysosomal storage disorder Aspartylglucosaminuria. Biochimica et biophysica acta. 2018; 1864:668–675. [PubMed: 29247835]

(A)

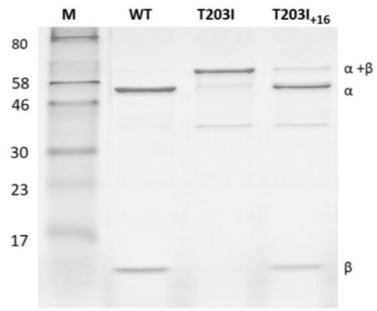

(B)

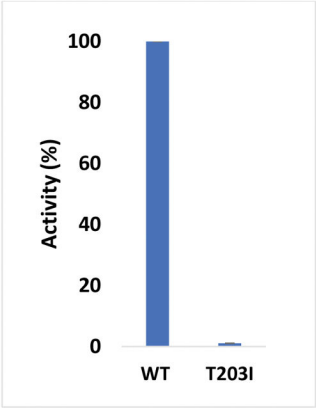

Figure 1. Autoproteolysis and hydrolysis activities of AGU T203I variant relative to the wild-type GA

(A) SDS-PAGE analysis of T203I variant. Lane M represents a mixture of molecular weight markers. Lanes WT and T203I are purified wild-type GA and AGU variant, respectively. To generate mature form of the T203I variant for kinetic studies (in Figure 4), freshly purified T203I precursor protein (lane T203I) was autoprocessed further *in vitro* by incubating for 16 hours at 37°C (lane $T203I_{+16}$) in a solution of 100 mM Tris, pH 7.5, 50 mM NaCl, and 10 mM EDTA. The precursor (α-β), and autocleaved subunits (α and β), are marked.

(B) Hydrolysis activity. The activity of wild-type GA is normalized to 100%. Data are average of three repeats with standard error shown as an error bar.

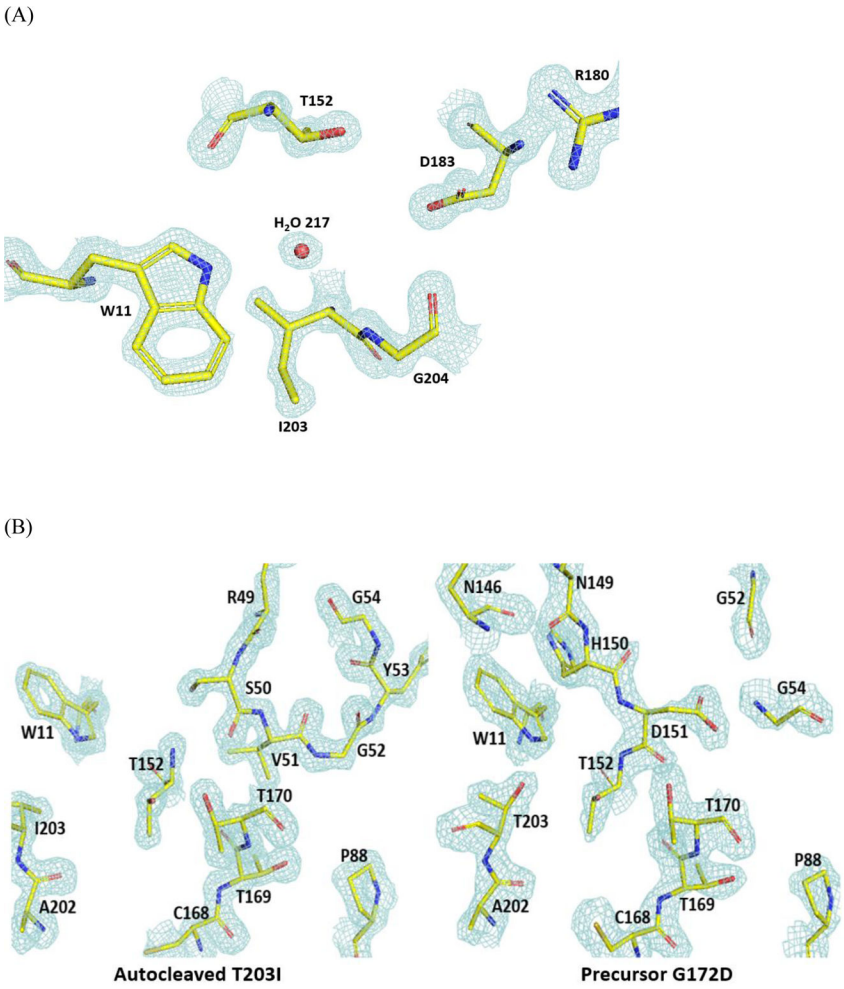

Figure 2. Electron density maps at the catalytic site of the T203I variant and another precursor variant

(A) Electron density map of the T203I variant. The cyan electron density corresponds to a $2F_o$-F_c type map at 1.6 Å resolution contoured at the 1.2-σ level. The hydrolytic nucleophile is the side-chain hydroxyl group of Thr152. Side chains of a few key active site residues are shown by atom type: yellow for carbon atoms, blue for nitrogen atoms, red for oxygen atoms. A bound water molecule (H_2O 217) is shown as a red sphere.

(B) Side-by-side comparison of electron density maps between the autocleaved T203I variant (left panel) and a precursor G172D variant published before (right panel) [16]. Color schemes are the same as in (A). Note the contrast between the well resolved density at T152 of the left panel, and the continuous density in the right panel for the P-loop (N149-T152). In the left panel, a surface loop (R49–G54) moves closer to T152, suggesting the P-loop had been autocleaved and released out of the space.

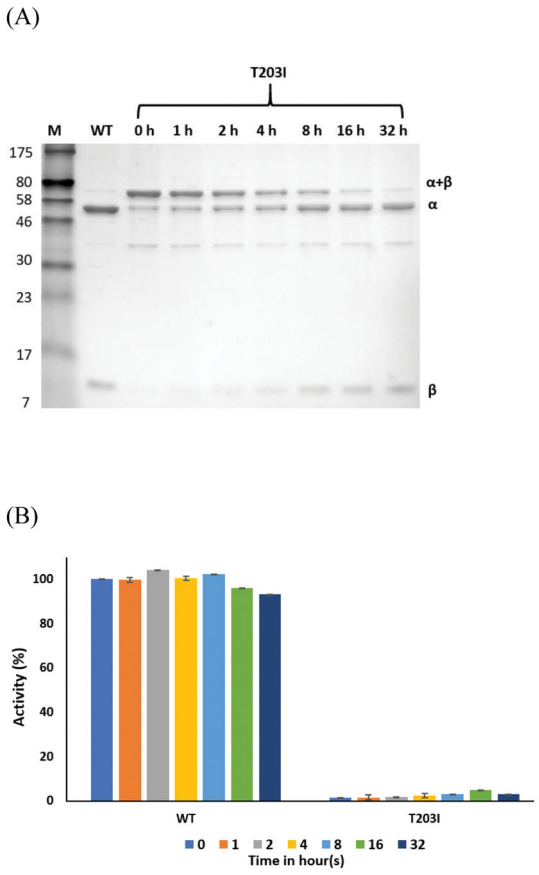

Figure 3. Time course of autoprocessing and corresponding hydrolysis activities of the T203I variant

(A) *In vitro* autoproteolysis analysis of the T203I variant. Autoproteolysis of purified T203I precursor protein was initiated by incubating the precursor at 37°C in a solution of 100 mM Tris, pH 7.5, 50 mM NaCl, and 10 mM EDTA. Aliquots were then removed at various time points, as indicated, and analyzed by SDS-PAGE. The precursor (α+β), autocleaved subunits (α and β) are marked. Lanes M and WT are a mixture of molecular weight markers and the wild- type GA, respectively.

(B) Enzyme hydrolysis assays. Purified AGU variant or wild-type GA proteins were incubated at 37 °C for 0–32 hours before measuring their hydrolase activities. See Experimental Procedures for detailed assay conditions. Activity of wild-type GA at 0 hr is normalized to 100%. Data are averages of 3 repeats ± standard errors.

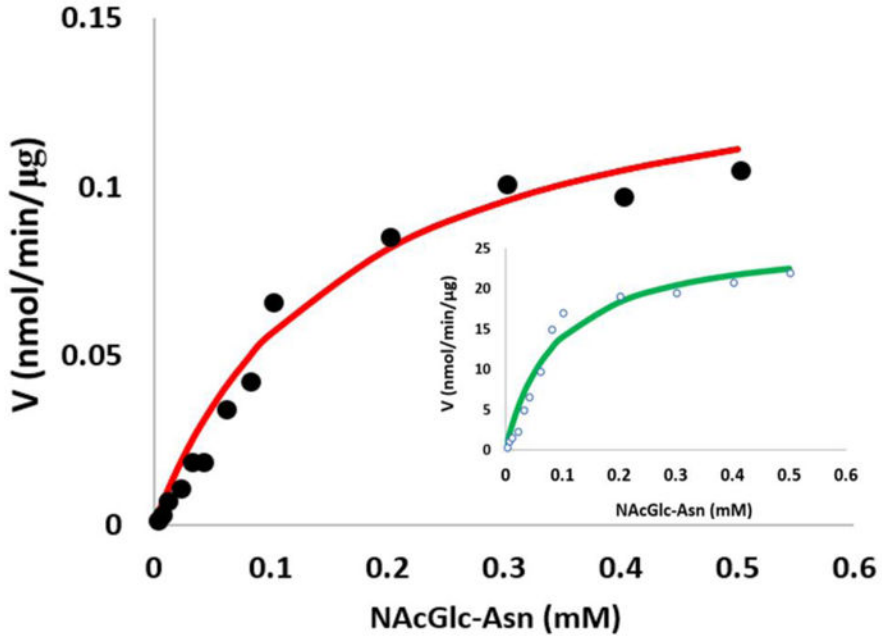

Figure 4. Kinetic analyses of the T203I mature hydrolase and the wild-type GA

Purified and *in vitro* autoprocessed T203I (Figure 1A, lane $T203I_{+16}$) as well as wild-type GA (0.04 µg) were used to determine the catalytic parameters K_M and kcat of hydrolysis of NAcGlc-Asn as substrate. Initial rates (V) were calculated based on reactions at three different time points, and are expressed in unit of nmoles/min/ug-protein for T203I variant (—●—) and the wild-type GA (inset, —○—).

(A)

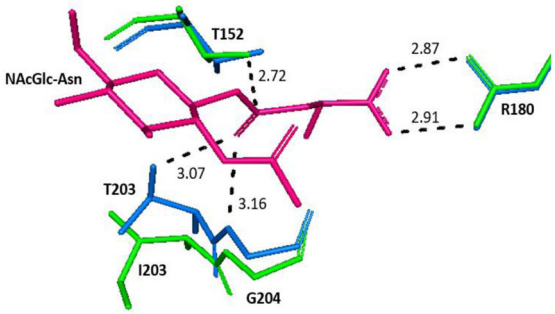

(B)

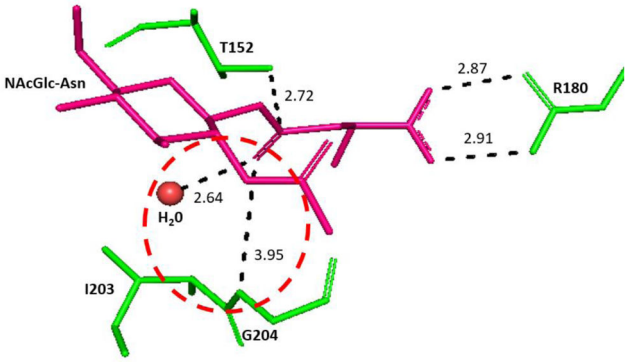

Figure 5. Model of T203I-substrate complex, and its hydrolytic mechanism

(A) Model of T203I-substrate complex. Hydrogen-bond contacts between the T203I variant and the modelled substrate NAcGlc-Asn. Active site residues of the T203I enzyme are shown in green, whereas NAcGlc-Asn substrate is shown in magenta. For comparison, the wild-type structure in complex with the substrate [31] is also shown in blue. Dash lines indicate the hydrogen-bond interactions with distances in angstroms (Å).

(B) The proposed catalytic mechanism. Hydrolysis of a substrate by T203I is carried out via Thr152 nucleophilic attack and an oxyanion hole made up with a nearby water molecule. Dashed lines represent hydrogen bond interactions with distances designated in angstroms. Large dotted circle represents the speculative oxyanion hole, and small red sphere represents a modeled water molecule slightly adjusted from the bound H_2O #217 (see Fig. 2).

Table 1

Different numbering schemes of two selected AGU variants and the model GA[a].

	Finnish AGU in this study	1st published AGU structure
− signal peptide	T234I	G203D
+ signal peptide	T257I	G226D
model GA (− signal peptide)	T203I	G172D

[a]Numbering differences are due to whether counting signal peptide and/or different lengths of the P-loop that connects the α and β subunits in the precursors.

Table 2

Crystallographic data collection and refinement statistics.

Resolution (Å)[a]	61.8-1.60 (1.63-1.60)
Space group	$P2_1$
Cell dimensions	
a, b, c (Å)	45.9, 96.5, 61.7
α, β, γ (°)	90.0 90.3 90.0
No. of molecules per asymmetric unit	2
I/sigma-I	16.8 (7.6)
Completeness (%)	97.3 (94.9)
R_{sym} (%)[b]	6.8 (20.0)
Structure refinement Resolution (Å)	20.0 - 1.60
No. of reflections	65,359
R_{work}[c]	0.169
R_{free}[d]	0.197
R.m.s. deviations[e]	
Bond-lengths (Å)	0.02
Bond-angles (°)	2.13
Ramachandran plot	
Most favored regions (%)	97.1
Additional allowed regions (%)	2.5
Outliners (%)	0.4
B-factors ($Å^2$)	
Main chain	11.6
Side chain	15.8
Water	20.4

[a] Numbers in parenthesis refer to the outermost resolution bin.

[b] $R_{sym} = \Sigma_h\Sigma_i | I_{hi} - I_h | / \Sigma_h\Sigma_i I_{hi}$ for the intensity (I) of i observation of reflection h.

[c] $R_{work} = \Sigma | F_{obs} - F_{calc} | / \Sigma | F_{obs} |$, where F_{obs} and F_{calc} are the observed and calculated structure factor amplitudes, respectively.

[d] R_{free} was calculated as R_{work}, but with 5% of the amplitudes chosen randomly and omitted from the start of refinement.

[e] R.m.s. deviations are deviations from ideal geometry.

Table 3

Kinetic parameters of wild-type GA and the AGU variant.

Enzyme	wild-type GA	AGU T203I variant
K_M (mM)	0.090±0.018	0.166±0.029
k_{cat} (sec^{-1})	14.18±0.99	0.08±0.01
k_{cat}/K_M ($sec^{-1}mM^{-1}$)	160	0.48